Low-Temperature Scanning Tunneling Microscopy Investigation of Epitaxial Growth of F16CuPc Thin Films on Ag(111)

ARTICLE *in* THE JOURNAL OF PHYSICAL CHEMISTRY C · JULY 2008

Impact Factor: 4.77 · DOI: 10.1021/jp8040007

3 AUTHORS:

Han Huang
National Chengchi University
81 PUBLICATIONS **1,844** CITATIONS
SEE PROFILE

Wei Chen
Chinese Academy of Sciences
874 PUBLICATIONS **13,856** CITATIONS
SEE PROFILE

Andrew Thye Shen Wee
National University of Singapore
607 PUBLICATIONS **11,331** CITATIONS
SEE PROFILE

Low-Temperature Scanning Tunneling Microscopy Investigation of Epitaxial Growth of $F_{16}CuPc$ Thin Films on Ag(111)

Han Huang, Wei Chen,* and Andrew Thye Shen Wee*

Department of Physics, National University of Singapore, 2 Science Drive 3, 117542, Singapore

Received: May 6, 2008; Revised Manuscript Received: June 11, 2008

In-situ low-temperature scanning tunneling microscopy (LT-STM) has been used to systematically investigate the epitaxial growth behaviors of copper hexadecafluorophthalocyanine ($F_{16}CuPc$) on Ag(111) from one monolayer to a few layers. At the monolayer regime, alternately arranged double-molecular-rows of $F_{16}CuPc$ form along the $[1\bar{1}0]$ direction of Ag(111). Within the same double-molecular-row, all $F_{16}CuPc$ molecules possess the same in-plane orientation. The growth in the second layer shows strong coverage dependence. At the initial growth stages of the second layer, isolated and rotated $F_{16}CuPc$ molecules pack along the $[1\bar{1}0]$ direction forming molecular dot-chains. Increasing the coverage leads to the appearance of densely packed and uniaxially oriented molecular nanoribbons comprising a few $F_{16}CuPc$ molecular rows packed exclusively along the $[1\bar{1}0]$ direction; this transits to a densely packed layer with all molecules having the same in-plane orientation. The growth of the third layer starts with the formation of densely packed molecular nanoribbons oriented along the $[1\bar{1}0]$ direction. Our results reveal that the growth of $F_{16}CuPc$ on Ag(111) adopts a layer-by-layer growth mode via $\pi-\pi$ stacking with their molecular π-plane oriented parallel to the substrate surface, stabilized through the interlayer dispersion forces.

Introduction

Organic semiconducting thin films comprising π-conjugated molecules have attracted much attention due to their promising applications in organic light emitting diodes (OLEDs),[1] solar cells,[2] and organic field effect transistors (OFETs).[3] Most devices require efficient charge transport or high carrier mobility through the active organic layers in order to optimize the device performance. Effective $\pi-\pi$ stacking of organic thin films can greatly facilitate the overlapping of π-orbitals between neighboring molecules, thereby resulting in high carrier mobility. For example, Li et al. recently reported that a high hole mobility close to 10 $cm^2\ V^{-1}\ s^{-1}$ can be achieved on titanyl phthalocyanine (TiOPc)-based thin film transistors,[4] arising from the close $\pi-\pi$ molecular contact. Such effective intermolecular $\pi-\pi$ interactions can also lead to the formation of a delocalized intermolecular band in the crystal, as shown in an angle-resolved photoemission spectroscopy (ARPES) study on crystalline films of uniaxially oriented *p*-sexiphenyl molecules.[5] As such, understanding the $\pi-\pi$ stacking mechanism of organic thin film growth is a subject of widespread interest.

The dependence of the growth behavior of organic thin films on factors such as molecular orientation, conformation, and three-dimentaional (3D) or 2D ordering are largely affected by the delicate balance between intermolecular and the molecule−substrate interfacial interactions.[6–10] The effective coupling between molecular orbitals and substrate valence or conduction bands plays a crucial role in determining the molecular orientation. The molecular orientation of organic thin films, i.e., standing-up versus lying-down, can be controlled by manipulating the surface electronic structure.[11–13] In contrast to the "atomic" systems of metals or inorganic semiconductors, organic molecules such as the widely used planar aromatic molecules are usually highly anisotropic. This can lead to the orientation-dependent intermolecular interactions that complicate the growth behavior. The interaction potential of inorganic adsorbates (adsorbate−adsorbate and adsorbate−substrate) is different from that of organic molecules, which is usually dominated by nonlocal dispersion forces.[14] Since many models describing the growth of inorganic materials are not directly applicable for organic materials, systematical investigations of the growth of organic molecules on well-defined single crystal substrates are needed to understand the unique growth mechanism of organic thin films, thereby facilitating the fabrication of films with well-controlled properties.

Copper hexadecafluorophthalocyanine ($F_{16}CuPc$) is a promising n-type semiconducting molecule[15] due to its remarkable chemical-, thermal-, and air-stability making it suitable for use in organic semiconductor devices, in particular n-channel and bipolar OFETs.[16] Previous studies focused on the growth of $F_{16}CuPc$ on inert dielectrics such as SiO_2.[17–19] On these substrates, $F_{16}CuPc$ molecules adopt a standing up configuration with their molecular π-plane oriented nearly perpendicular to the substrate surface. In contrast, on single crystalline metal substrates such as Cu(111) and Ag(111), $F_{16}CuPc$ molecules lie flat as suggested by scanning tunneling microscopy (STM) studies,[20,21] but with significant molecular distortion as revealed by an X-ray standing waves (XSW) investigation.[22] In this paper, we present a low-temperature STM (LT-STM) study of the epitaxial growth behavior of $F_{16}CuPc$ thin films on Ag(111) with coverage ranging from one monolayer to a few layers. The specific adsorption sites at the initial growth stages of each layer, as well as the molecular packing and orientation are systematically investigated.

Experimental Section

The experiments were carried out in a custom-built multichamber ultrahigh vacuum (UHV) system housing an Omicron LT-STM with the base pressure better than 6.0×10^{-11}

* Corresponding authors. E-mail: (W.C.) phycw@nus.edu.sg; (A.T.S.W.) phyweets@nus.edu.sg.

10.1021/jp8040007 CCC: $40.75
Published on Web 07/16/2008

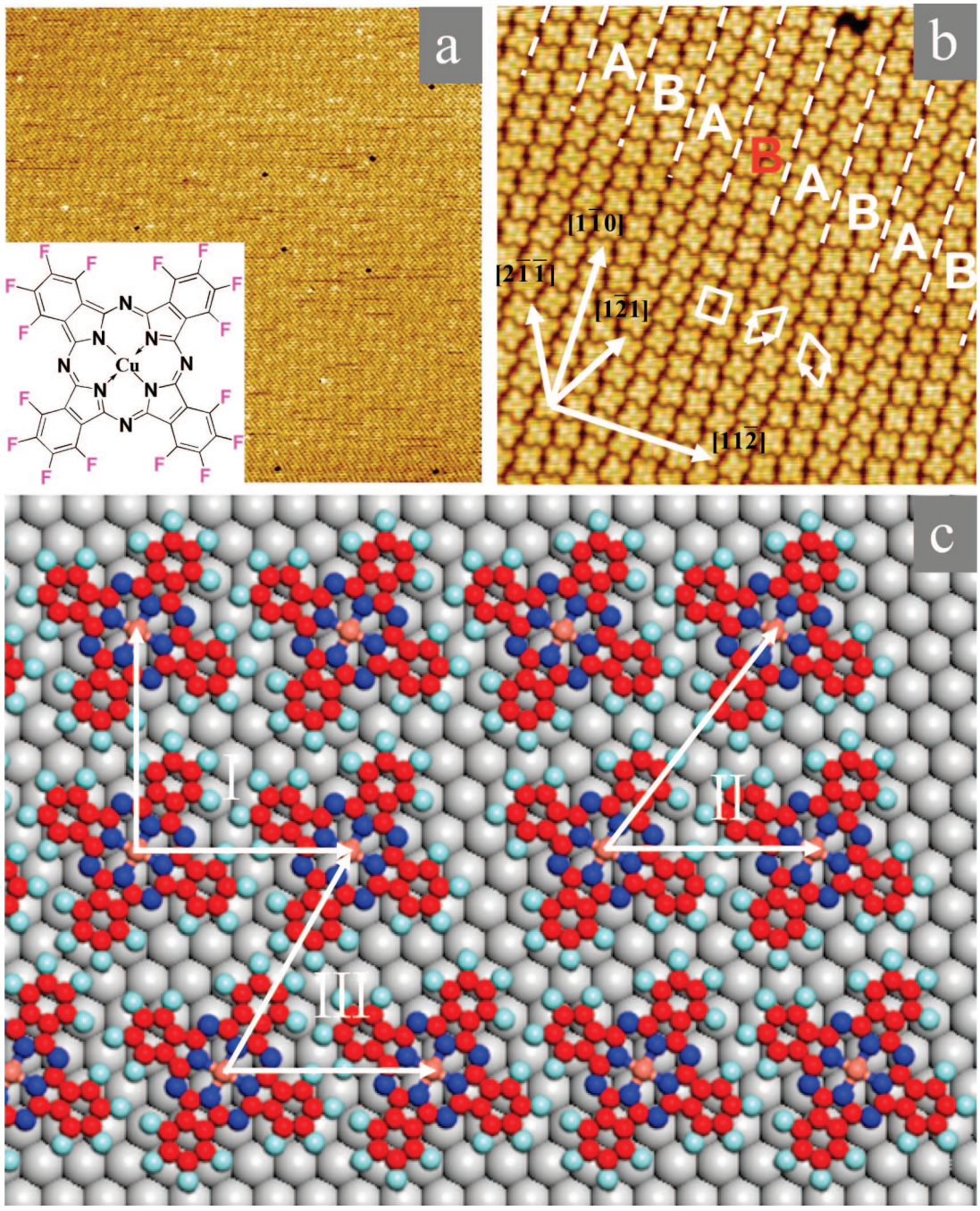

Figure 1. (a) Large scale STM image (200 nm × 200 nm, V_T = 1.9 V) of monolayer F_{16}CuPc on Ag(111), the insert showing the molecular structure of F_{16}CuPc. (b) Corresponding molecularly resolved STM image (30 nm × 30 nm, V_T = 1.9 V). The azimuths of the substrate are shown by a set of arrows. Three unit cells are highlighted by three white tetragons respectively. Different domains are separated by dashed lines and labeled by "A" and "B". (c) Proposed models of three kinds of unit cells of F_{16}CuPc on Ag(111).

mbar.[23,24] All the STM images were recorded in constant current mode using chemically etched tungsten (W) tips at 77 K. Ag(111) was cleaned *in situ* by several cycles of Ar^+ sputtering and subsequent annealing at ~800 K. The sample's cleanliness was verified by STM and low-energy electron diffraction (LEED) measurements. Before evaporation, F_{16}CuPc (Sigma-Aldrich) powder was purified twice by vacuum gradient sublimation (Crenphys). After overnight degassing at 600 K, F_{16}CuPc was evaporated from a double-head K-cell (Crenphys) onto the Ag(111) substrate at room temperature (RT) in the growth chamber (better than 2×10^{-10} mbar). The deposition rate was 0.03 ML/min at 615 K, calibrated by a Quartz Crystal Microbalance (QCM) and further confirmed by large-scale STM images. After growth, the sample was transferred to the L-N_2 cooled STM sample stage (77K) for imaging.

Results and Discussion

(i) F_{16}CuPc Monolayer on Ag(111). At the initial growth stage on Ag(111), F_{16}CuPc molecules predominantly decorate the step edges (data not shown), assembling into single-molecular chains along the step edges.[20] Upon increasing the coverage to 0.5 ML, the molecules nucleate into single-layered islands with well-ordered molecular arrangements on terraces. The monolayer retains the same supramolecular packing structure at 1 ML coverage. Figure 1a is a representative STM image of a F_{16}CuPc monolayer on a large Ag(111) terrace. The

molecular structure is shown in the inset of Figure 1a. The images indicate a long-range ordered monolayer structure with very few missing molecular vacancy defects (dark spots). The limited molecular surface diffusion at 77 K facilitates STM imaging with submolecular resolution. A typical high-resolution STM image is shown in Figure 1b. The four-leaf feature with a central dark hole represents a single $F_{16}CuPc$ molecule. Similar to other phthalocyanine molecules,[25] the four leaves are assigned to the four F-substituted peripheral benzene rings and the center dark hole to the Cu atom. $F_{16}CuPc$ adopts a lying down configuration with its molecular π-plane parallel to the surface, arising from the effective coupling between d-band electrons in Ag and the π-orbitals in $F_{16}CuPc$.[26–28]

Figure 1b shows that the $F_{16}CuPc$ molecules assemble along the $[1\bar{1}0]$ direction of Ag(111), forming well-ordered molecular rows. This is different with that of $F_{16}CoPc$ on Au(111) at RT, where no ordered structure was observed.[25b] Close inspection reveals that the molecules in two neighboring molecular rows adopt the same in-plane orientation, and is referred to as a double-molecule-row. Two types of double-molecule-rows dominate the $F_{16}CuPc$ monolayer on Ag(111), and they are labeled "A" and "B" in Figure 1b. One diagonal of the square molecule in row B is aligned along the $[1\bar{2}1]$ direction of Ag(111); while one diagonal of the molecule in row A is along the $[2\bar{1}\bar{1}]$ direction. Such long-range ordered double-molecule-rows of $F_{16}CuPc$ have not been observed on other substrates such as Au(111) or Cu(111).[20a,21] Although on monolayer CoPc covered Au(111) VOPc molecules can form ordered structure with double rows of alternating rotational orientation,[32b] the formation mechanism is not well-explained yet. More experimental and theoretical works are currently underway to clarify this issue.

The intermolecular distance along the molecular row is 15.0 ± 0.1 Å, close to 5 times the lattice constant of Ag(111) ($a_1 = 2.89$Å). Along the direction perpendicular to the molecular rows, i.e., the $[11\bar{2}]$ direction, the average inter-row distance is about 15.2 ± 0.1 Å, close to 3 times the lattice constant of Ag(111) along that direction ($\sqrt{3}a_1 = 5.05$Å). The two lengths are consistent with the van der Waals dimension of isolated $F_{16}CuPc$ molecules.[18,19] On the basis of the relative longitudinal translation in the molecular row direction, three possible commensurable unit cells are proposed. As shown in Figure 1c, the three unit cells are denoted, respectively, by the following matrices:

$$\mathrm{I}\begin{pmatrix}5 & 0\\ 2 & 6\end{pmatrix}, \qquad \mathrm{II}\begin{pmatrix}5 & 0\\ 1 & 6\end{pmatrix}, \qquad \mathrm{III}\begin{pmatrix}5 & 0\\ 0 & 6\end{pmatrix}$$

All three unit cells have the same footprint of around 216.4 Å^2, comparable to that of an isolated $F_{16}CuPc$ molecule of about 210 Å^2.[18,19] This suggests that the $F_{16}CuPc$ monolayer is in registry with Ag(111).

As highlighted by the white square in Figure 1b, a double-molecule-row labeled by a red "B" has a square unit cell, corresponding to type I unit cell. The other double-molecule-row in Figure 1b, labeled as a white "A" and "B", have the same oblique unit cells with an acute angle of about 60° with respect to each other, as highlighted by the two equivalent parallelograms. They correspond to the type III unit cell. However, the proposed type II unit cell has not been identified in the $F_{16}CuPc$ monolayer on Ag(111) after inspecting many STM images. It is worth noting that the double-molecular-row A and B are mirrored structures with a small lateral displacement. Therefore, it is not a simple mirror symmetry but a glide-mirror symmetry in the first $F_{16}CuPc$ layer on Ag(111).[29,30]

(ii) Second layer $F_{16}CuPc$ on Ag(111). The initial growth behavior of the second layer is different from that of the first layer. Instead of forming a close packed layer, isolated $F_{16}CuPc$ molecules align along the molecular row direction of the underlying first layer, i.e., the $[1\bar{1}0]$ direction of Ag(111), forming molecular dot-chains. Figure 2a shows a typical 230×230 nm^2 STM image of 1.2 ML $F_{16}CuPc$ on Ag(111). The corresponding high resolution image is shown in Figure 2b. Similar to the first layer of $F_{16}CuPc$ where the molecules in the neighboring double-molecular-row adopt different in-plane orientations, the molecules in the second layer also possess two different in-plane orientations. It is obvious that the isolated $F_{16}CuPc$ molecules adsorb directly on top of the first layer molecules with the molecular π-planes parallel to Ag(111). (more details can be found in Supporting Information) This confirms the $\pi-\pi$ stacking between the first two $F_{16}CuPc$ layers, which enhances interlayer π-orbital overlapping and facilitates efficient charge transport along the $\pi-\pi$ stacking direction.[4]

Figure 2c is an enlarged STM image showing the epitaxial relationship between the $F_{16}CuPc$ molecules in the first two layers. The inset in the upper-right corner highlights the molecular arrangement in the underlying first layer. Close inspection reveals that the four lobes of the upper molecule are not stacked directly above those of the molecule underneath but are rotated by an angle of $\theta \approx 45°$. The interlayer interactions between the first two layers are dominated by intermolecular $\pi-\pi$ interactions, which can be decomposed into dispersion and electrostatic forces. It has been reported that the repulsive intermolecular electrostatic force or the quadruple-quadruple interaction destabilizes the parallel benzene dimer.[31] The parallel configuration refers to the benzene dimer of one molecule stacking directly above another molecule without any in-plane displacement. As such, the observed molecular rotation between the second and first layer of $F_{16}CuPc$ can be understood in terms of minimization of the repulsive intermolecular electrostatic force.[20] During STM imaging, all the isolated molecules are immobilized and no diffusion of these molecules were observed. This suggests that the rotated adsorption geometry is a stable configuration for the isolated second layer $F_{16}CuPc$ molecules. In particular, these isolated $F_{16}CuPc$ molecules assemble along the $[1\bar{1}0]$ direction of Ag(111), i.e., the molecular packing direction of the underlying first layer molecular rows, forming well-aligned molecular dot-chains.

The line-profiles in Figure 2d show that the intermolecular distance between the neighboring isolated $F_{16}CuPc$ molecules (the upper red line) along the $[1\bar{1}0]$ direction of Ag(111) is double ($2a$) or triple ($3a$) the intermolecular distance (a) of the first molecular layer along the same direction (the lower blue line). Larger intermolecular separations of integer multiples of a can also be found. For the rotated second layer $F_{16}CuPc$ molecules, the projected molecular length along the $[1\bar{1}0]$ direction is larger than a as can be seen in the geometrical rotation of a square. It precludes the possibility of two rotated $F_{16}CuPc$ molecules being adsorbed on top of two adjacent molecules in the first layer along the $[1\bar{1}0]$ direction. Otherwise, significant overlapping between these two rotated molecules would occur inducing large repulsive forces between them. This is consistent with the line profile measurements. The minimum intermolecular distance between the isolated second layer $F_{16}CuPc$ along the $[1\bar{1}0]$ direction is $2a$, not a. The interlayer separation is measured to be 2.7 ± 0.1 Å, slightly smaller than the previously reported intermolecular distance of cofacially oriented $F_{16}CuPc$ molecules of around 3.1 Å, determined by the X-ray diffraction measurements.[22] This discrepancy is attributed to the fact that the STM image is a convolution of both electronic and geometric properties of the surface.[32]

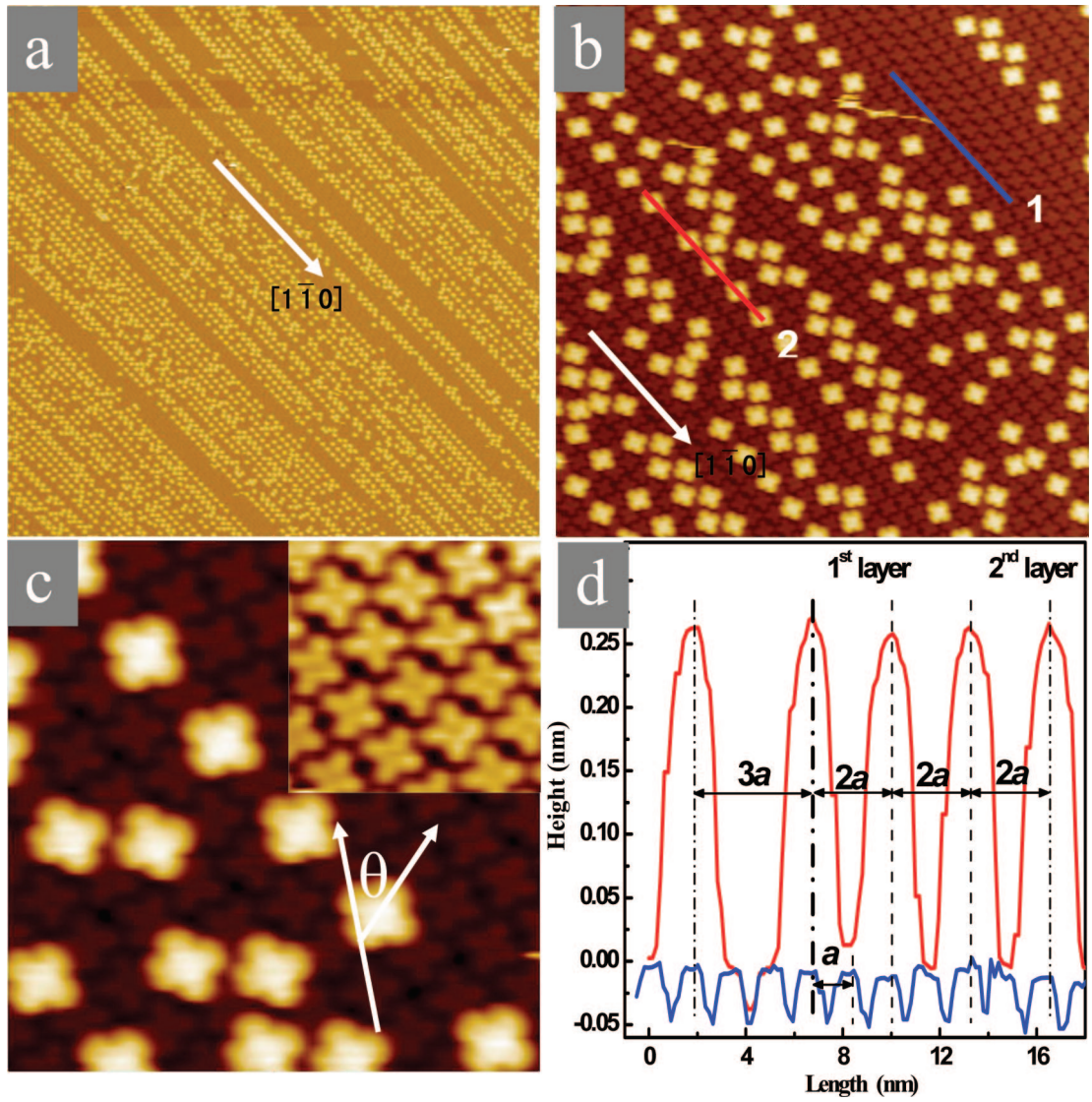

Figure 2. (a) Large scale STM image (230 nm × 230 nm, V_T = 2.9 V) and (b) corresponding close-up (50 nm × 50 nm, V_T = 2.8 V) of around 0.2 ML more F_{16}CuPc molecules deposited on the monolayer F_{16}CuPc covered Ag(111) surface. (c) Enlarged STM image (15 nm × 15 nm, V_T = 2.8 V) from panel b showing the relative rotation between molecules in the first two layers. (d) Line profiles taken along Lines 1 (blue) and 2 (red) in panel b. the intermolecular distance of molecules in the first layer is defined as "*a*".

Since the minimum intermolecular separation between two isolated second layer F_{16}CuPc molecules along the [1$\bar{1}$0] direction is 2*a*, the second layer coverage exclusively comprising the isolated and rotated F_{16}CuPc molecules is limited to be half of that in the first layer at a total coverage of 1.5 ML. Additional incoming F_{16}CuPc molecules will either stack on top of these isolated second layer molecules to form the third layer or induce a structural rearrangement of the isolated molecules to a densely packed second layer. In our experiments, we observe the latter case. Beyond 1.5 ML coverage, densely packed molecular nanoribbons along the [1$\bar{1}$0] direction are formed as shown in Figure 3a. Figure 3b displays a STM image of a nanoribbon in the second layer consisting of three molecular rows with isolated molecules located nearby. It is worth noting that all F_{16}CuPc molecules in this three-molecule-wide nanoribbon adopt the same in-plane orientation and a $\pi-\pi$ stacking along the direction perpendicular to the molecular plane. The interlayer electrostatic repulsion force can therefore be reduced by a small lateral displacement and molecular in-plane rotation between the molecules in the first and second layers. Such $\pi-\pi$ stacking between the first two layers is mainly stabilized through the interlayer dispersion forces.

When the coverage increases to 1.9 ML, as shown in Figure 3c, the second layer is dominated by the closely packed layer, leaving some unsaturated areas with molecular dots. Figure 3d is a high resolution image of the closely packed second F_{16}CuPc layer, revealing that all molecules possess the same in-plane orientation. This is different from the alternating arrangement of double-molecule-row in the first layer of F_{16}CuPc on Ag(111). The molecular plane of F_{16}CuPc in the second layer is also oriented parallel to the substrate surface. Upon increasing the coverage to 2 ML, the second layer is fully saturated.

(iii) Third layer of F_{16}CuPc on Ag(111). After the second layer is fully completed, impinging molecules nucleate into densely packed molecular nanoribbons along the [1$\bar{1}$0] direction with uniform in-plane orientations. A typical large scale STM image is shown in Figure 4a. Three molecular nanoribbons each comprising five molecular rows form on top of the second layer of densely packed F_{16}CuPc. Figure 4b shows an STM image of a F_{16}CuPc nanoribbon (the third layer) comprising 11 molecular rows. All the molecules have the same in-plane orientations with some lateral displacement along the ribbon. The inset at the lower-right corner of Figure 4b shows the corresponding high-resolution STM image at the right edge of the ribbon, clearly

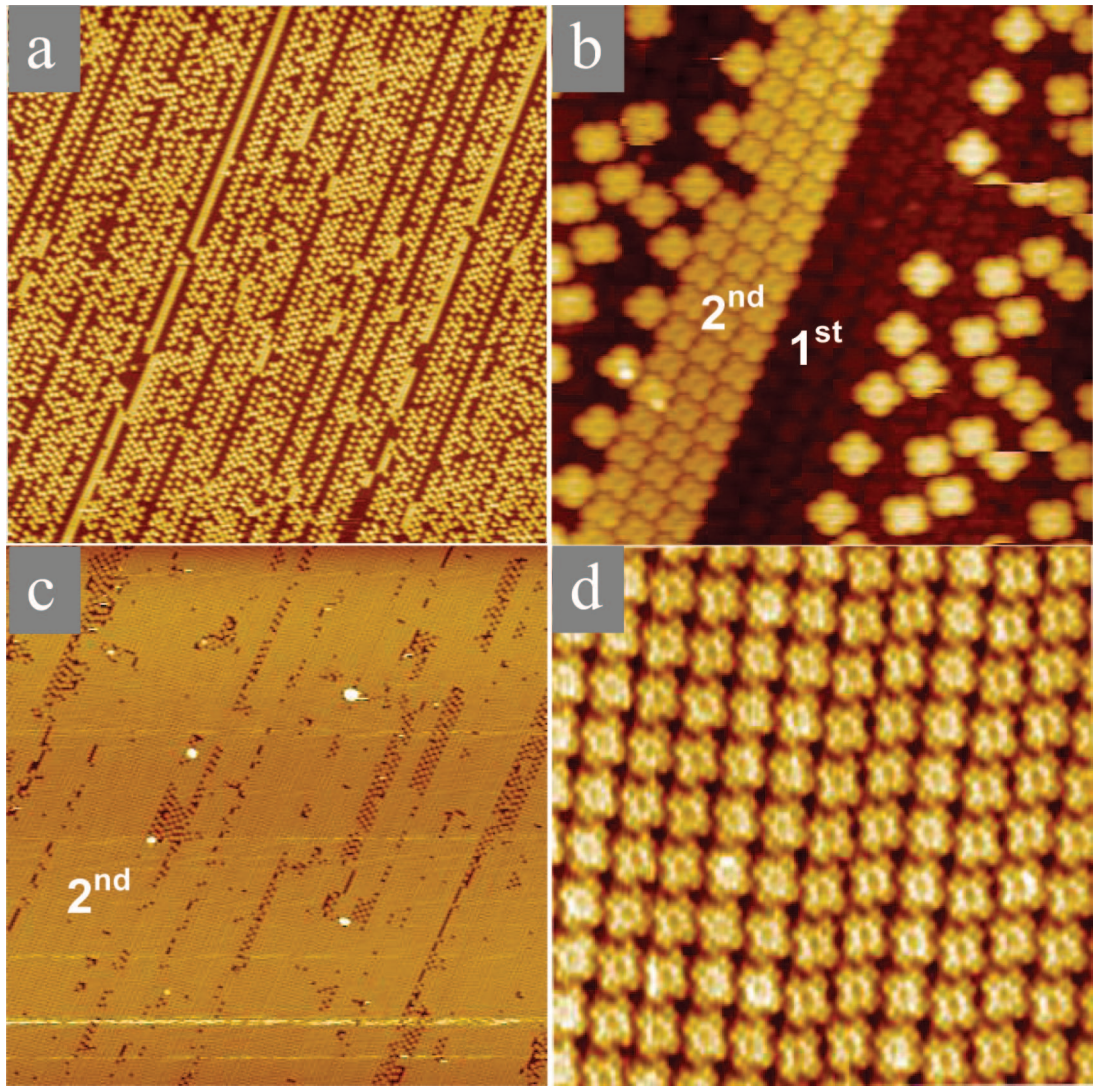

Figure 3. (a and c) Large scale (200 nm × 200 nm, $V_T = 2.6$ V) and (b) (26 nm × 26 nm, $V_T = 2.8$ V) and (d) (17 nm × 17 nm, $V_T = 2.6$ V) submolecularly resolved STM images of 1.5 ML (panel a, b) and 1.9 ML (panel c, d) $F_{16}CuPc$ on Ag(111), respectively.

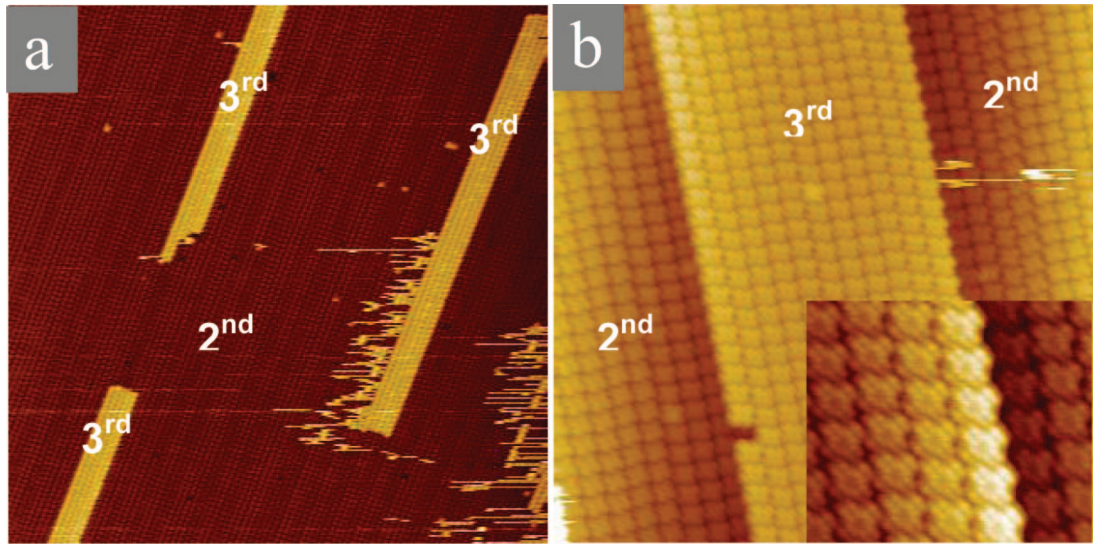

Figure 4. (a) Large scale STM image (150 nm × 150 nm, $V_T = 2.5$ V) and(b) a close-up (40 nm × 40 nm, $V_T = 2.8$ V) of the nanoribbons of the third layer $F_{16}CuPc$ on top of the second layer. The inset in panel b shows internal molecular structure.

revealing the $F_{16}CuPc$ internal molecular structures. As with CuPc,[25] the center Cu atom appears as a dark hole. It is surrounded by eight bright spots, which correspond to the eight N atoms in the center ring close to the Cu atom. The outmost bright dots are attributed to the F-substituted periphery benzene rings.[20,21] This clearly suggests that the third layer molecules

adsorb flat atop the second layer. Our results reveal a layer-by-layer growth mode via $\pi-\pi$ stacking for F_{16}CuPc on Ag(111).

Conclusion

The growth behavior of F_{16}CuPc thin films on Ag(111) from one monolayer to a few layers have been systematically investigated using *in situ* LT-STM, revealing a layer-by-layer growth mode via $\pi-\pi$ stacking. At the monolayer regime, an alternately arranged double-molecular-rows of F_{16}CuPc form along the $[1\bar{1}0]$ direction of Ag(111). Within the same double-molecular-row, all F_{16}CuPc molecules possess the same in-plane orientation. The molecules in the neighboring double-molecular-rows, however, adopt different in-plane orientations. In the second layer, the growth is significantly coverage-dependent. At the initial growth stages of the second layer, isolated F_{16}CuPc molecules pack along the $[1\bar{1}0]$ direction, forming molecular dot-chains. The intermolecular distance between these isolated F_{16}CuPc are integer multiples of the underlying first layer F_{16}CuPc along the molecular row packing direction. Increasing the coverage to 1.5 ML leads to the appearance of densely packed and uniaxially oriented molecular nanoribbons comprising a few F_{16}CuPc molecular rows packed exclusively along the $[1\bar{1}0]$ direction. Increasing the coverage to 2.0 ML results in a densely packed layer with all molecules having identical in-plane orientation. In contrast to the second layer, the growth of the third layer starts with the formation of densely packed molecular nanoribbons oriented along the $[1\bar{1}0]$ direction. Such detailed investigation of the epitaxial growth behavior of F_{16}CuPc on Ag(111) can help us better understand the $\pi-\pi$ stacking mechanism of π-conjugated planar molecules on surfaces. This will enable us to better control the film properties such as supramolecular packing and molecular orientation for their applications in organic electronic devices, in particular, air-stable n-channel OFETs based on F_{16}CuPc or bipolar OFETs based on the combination of F_{16}CuPc with CuPc or other p-type molecules.

Acknowledgment. Dr. W. Chen acknowledges the financial support by LKY PDF fellowship. Authors acknowledge the support from the A*STAR Grant R-398-000-036-305 and ARF Grant R-144-000-196-112.

Supporting Information Available: Molecular-resolved STM images of the molecular-dot chains of the 2nd layer F_{16}CuPc on Ag(111). This material is available free of charge via the Internet at http://pubs.acs.org.

References and Notes

(1) (a) Tang, C. W.; Van Slyke, S. A. *Appl. Phys. Lett.* **1987**, *51*, 913. (b) Forrest, S. R. *Nature* **2004**, *428*, 911.

(2) (a) Blom, P. W. M.; Mihailetchi, V. D.; Koster, L. J. A.; Markov, D. E. *Adv. Mater.* **2007**, *19*, 1551. (b) Forrest, S. R. *MRS Bulletin* **2005**, *30*, 28.

(3) (a) Crone, B.; Dodabalapur, A.; Lin, Y. Y.; Filas, R. W.; Bao, Z.; LaDuca, A.; Sarpeshkar, R.; Katz, H. E.; Li, W. *Nature* **2000**, *403*, 521. (b) Dimitrakopoulos, C. D.; Malenfant, P. R. L. *Adv. Mater.* **2002**, *14*, 99.

(4) Li, L. Q.; Tang, Q. X.; Li, H. X.; Yang, X. D.; Hu, W. P.; Song, Y. B.; Shuai, Z. G.; Xu, W.; Liu, Y. Q.; Zhu, D. B. *Adv. Mater.* **2007**, *19*, 2613.

(5) Koller, G.; Berkebile, S.; Oehzelt, M.; Puschnig, P.; Ambrosch-Draxl, C.; Netzer, F. P.; Ramsey, M. G. *Science* **2007**, *317*, 351.

(6) (a) Chen, W.; Huang, H.; Chen, S.; Chen, L.; Zhang, H. L.; Gao, X. Y.; Wee, A. T. S. *Appl. Phys. Lett.* **2007**, *91*, 114102. (b) Chen, W.; Huang, H.; Chen, S.; Gao, X. Y.; Wee, A. T. S. *J. Phys. Chem. C.* **2008**, *112*, 5036. (c) Chen, W.; Chen, S.; Huang, H.; Qi, D. C.; Gao, X. Y.; Wee, A. T. S. *Appl. Phys. Lett.* **2008**, *92*, 063308.

(7) (a) Cheng, Z. H.; Gao, L.; Deng, Z. T.; Liu, Q.; Jiang, N.; Lin, X.; He, X. B.; Du, S. X.; Gao, H. J. *J. Phys. Chem. C* **2007**, *111*, 2656. (b) Cheng, Z. H.; Gao, L.; Deng, Z. T.; Jiang, N.; Liu, Q.; Shi, D. X.; Du, S. X.; Guo, H. M.; Gao, H. J. *J. Phys. Chem. C* **2007**, *111*, 9240.

(8) (a) Abel, M.; Oison, V.; Koudia, M.; Maurel, C.; Katan, C.; Porte, L. *ChemPhysChem.* **2006**, *7*, 82. (b) Koudia, M.; Abel, M.; Maurel, C.; Bliek, A.; Catalin, D.; Mossoyan, M.; Mossoyan, J. C.; Porte, L. *J. Phys. Chem. B* **2006**, *110*, 10058. (c) Oison, V.; Koudia, M.; Abel, M.; Porte, L. *Phys. Rev. B* **2007**, *75*, 035428.

(9) Theobald, J. A.; Oxtoby, N. S.; Phillips, M. A.; Champness, N. R.; Beton, P. H. *Nature* **2003**, *424*, 1029.

(10) (a) Rosei, F.; Schunack, M.; Naitoh, Y.; Jiang, P.; Gourdon, A.; Lægsgaard, E.; Stensgaard, I.; Joachim, C.; Besenbacher, F. *Prog. Surf. Sci.* **2003**, *71*, 95. (b) Chen, W.; Wee, A. T. S. *J. Phys. D: Appl. Phys.* **2007**, *40*, 6287.

(11) (a) Chen, W.; Huang, C.; Gao, X. Y.; Wang, L.; Zhen, C. G.; Qi, D. C.; Chen, S.; Zhang, H. L.; Loh, K. P.; Chen, Z. K.; Wee, W. T. S. *J. Phys. Chem. B.* **2006**, *110*, 26075. (b) Chen, W.; Chen, S.; Qi, D. C.; Gao, X. Y.; Chen, Z. K.; Wee, W. T. S. *Adv. Funct. Mater.* **2007**, *17*, 1339. (c) Chen, W.; Wang, L.; Qi, D. C.; Chen, S.; Gao, X. Y.; Wee, A. T. S. *Appl. Phys. Lett.* **2006**, *88*, 184102.

(12) (a) Duhm, S.; Heimel, G.; Salzmann, I.; Glowatzkl, H.; Johnson, R. L.; Vollmer, A.; Rabe, J. P.; Koch, N. *Nat. Mater.* **2008**, *7*, 326. (b) Ivanco, J.; Winter, B.; Netzer, T. R.; Ramsey, M. G. *Adv. Mater.* **2003**, *15*, 1812. (c) Winter, B.; Berkebile, S.; Ivanco, J.; Koller, G.; Netzer, F. P.; Ramsey, M. G. *Appl. Phys. Lett.* **2006**, *88*, 253111.

(13) Thayer, G. E.; Sadowski, J. T.; zu Heringdorf, F. M.; Sakurai, T.; Tromp, R. M. *Phys. Rev. Lett.* **2005**, *95*, 256106.

(14) Schreiber, F. *Phys. Status Solidi A:* **2004**, *201*, 1037.

(15) Bao, Z.; Lovinger, A. J.; Brown, J. *J. Am. Chem. Soc.* **1998**, *120*, 207.

(16) (a) Klauk, H.; Zschieschang, U.; Pflaum, J.; Halik, M. *Nature* **2007**, *445*, 745. (b) Wang, J.; Wang, H. B.; Yan, X. J.; Huang, H. C.; Yan, D. H. *Appl. Phys. Lett.* **2005**, *87*, 093507. (c) Wang, J.; Wang, H. B.; Yan, X. J.; Huang, H. C.; Jin, D.; Shi, J. W.; Tang, Y. H.; Yan, D. H. *Adv. Funct. Mater.* **2006**, *16*, 824. (d) Lau, K. M.; Tang, J. X.; Sun, H. Y.; Lee, C. S.; Lee, S. T.; Yan, D. H. *Appl. Phys. Lett.* **2006**, *88*, 173513.

(17) Osso, J. O.; Schreiber, F.; Kruppa, V.; Dosch, H.; Garriga, M.; Alonso, M. I.; Cerdeira, F. *Adv. Funct. Mater.* **2002**, *12*, 455.

(18) Osso, J. O.; Schreiber, F.; Alonso, M. I.; Garriga, M.; Barrena, E.; Dosch, H. *Org. Electron.* **2004**, *5*, 135.

(19) de Oteyza, D. G.; Barrena, E.; Osso, J. O.; Sellner, S.; Dosch, H. *J. Am. Chem. Soc.* **2006**, *128*, 15052.

(20) (a) Wakayama, Y. *J. Phys. Chem. C* **2007**, *111*, 2675. (b) Barlow, D. E.; Scudiero, L.; Hipps, K. W. *Langmuir* **2004**, *20*, 4413.

(21) Barrena, E.; de Oteyza, D. G.; Dosch, H.; Wakayama, Y. *ChemPhyChem.* **2007**, *8*, 1915.

(22) Gerlach, A.; Schreiber, F.; Sellner, S.; Dosch, H.; Vartanyants, I. A.; Cowie, B. C. C.; Lee, T. L.; Zegenhagen, J. *Phys. Rev. B* **2005**, *71*, 205425.

(23) Zhang, H. L.; Chen, W.; Chen, L.; Huang, H.; Wang, X. S.; Yuhara, J.; Wee, A. T. S. *Small* **2007**, *3*, 2015.

(24) Huang, H.; Chen, W.; Chen, L.; Zhang, H. L.; Wang, X. S.; Bao, S. N.; Wee, A. T. S. *Appl. Phys. Lett.* **2008**, *92*, 023105.

(25) (a) Lu, X.; Hipps, K. W.; Wang, X. D.; Mazur, U. *J. Am. Chem. Soc.* **1996**, *118*, 7197. (b) Scudiero, L.; Hipps, K. W.; Barlow, D. E. *J. Phys. Chem. B* **2003**, *107*, 2903.

(26) (a) Ferretti, A.; Baldacchini, C.; Calzolari, A.; Di Felice, R.; Ruini, A.; Molinari, E.; Betti, M. G. *Phys. Rev. Lett.* **2007**, *99*, 046802. (b) Kraft, A.; Temirov, R.; Henze, S. K. M.; Soubatch, S.; Rohlfing, M.; Tautz, F. S. *Phys. Rev. B.* **2006**, *74*, 041402. (c) Temirov, R.; Soubatch, S.; Luican, A.; Tautz, F. S. *Nature* **2006**, *444*, 350.

(27) Huang, H.; Zhang, H. J.; Botters, B.; Chen, Q.; Mao, H. Y.; He, P.; Bao, S. N. *J. Chem. Phys.* **2006**, *24*, 054716.

(28) Song, F.; Huang, H.; Dou, W. D.; Zhang, H. J.; Hu, Y. W.; Qian, H. Q.; Li, H. Y.; He, P. M.; Bao, S. N.; Chen, Q.; Zhou, W. Z. *J. Phys.: Condens. Matter* **2007**, *19*, 136002.

(29) (a) Sellam, F.; Schmitz-Hubsch, T.; Toerker, M.; Mannsfeld, S.; Proehl, H.; Fritz, T.; Leo, K.; Simpson, C.; Mullen, K. *Surf. Sci.* **2001**, *478*, 113. (b) Kang, J. H.; Toomes, R. L.; Polcik, M.; Kittel, M.; Hoeft, J. H.; Efstathiou, V.; Woodruff, D. P.; Bradshaw, A. M. *J. Chem. Phys.* **2003**, *118*, 6059.

(30) Song, F.; Dou, W. D.; Huang, H.; Li, H. Y.; He, P.; Bao, S. N. *Chem. Phys. Lett.* **2008**, *452*, 275.

(31) Tsuzuki, S.; Honda, K.; Uchimaru, T.; Mikami, M.; Tanabe, K. *J. Am. Chem. Soc.* **2002**, *124*, 104.

(32) (a) Hansma, P. K.; Tersoff, J. *J. Appl. Phys.* **1987**, *61*, R1. (b) Barlow, D. E.; Scudiero, L.; and Hipps, K. W. *Ultramicroscopy* **2003**, *97*, 47.

JP8040007